Chapter 4
Numerical Methods for Solving Boundary-Value Problems

4.1 Variational Formulation in Two-Dimensional Magnetostatics

Let the following magnetostatic boundary-value problem be considered

$$-\overline{\nabla}\cdot\left(\mu^{-1}\overline{\nabla}A\right)=J \text{ in } \Omega \tag{4.1}$$

$$A=0 \quad \text{along } \Gamma_D \tag{4.2}$$

$$\frac{\partial A}{\partial n}=0 \quad \text{along } \Gamma_N \tag{4.3}$$

where $\Gamma_D \cup \Gamma_N = \Gamma$ is the boundary of the two-dimensional simply-connected domain Ω, while A and μ are vector potential and magnetic permeability, respectively. Assuming rectangular coordinates, one has $\overline{A}=A\bar{i}_z$ and $\overline{J}=J\bar{i}_z$, whereas in cylindrical coordinates $\overline{A}=A\bar{i}_\varphi$ and $\overline{J}=J\bar{i}_\varphi$.

It is assumed that J and the second derivative of A are continuous in Ω so that the integral of both sides of (4.1) exists.

A way to approximate the solution to (4.1)–(4.3) is to relax the differential formulation of the boundary-value problem (weak formulation); to this end, the average of both sides of (4.1), weighted by a suitable test function, is considered. Accordingly, if u is a test function which is continuous up to its second derivative, from (4.1) one has

$$u\left(\overline{\nabla}\cdot\left(\mu^{-1}\overline{\nabla}A\right)+J\right)=0 \tag{4.4}$$

and, by integrating over the domain, one gets

$$\int_\Omega u\overline{\nabla}\cdot\left(\mu^{-1}\overline{\nabla}A\right)d\Omega+\int_\Omega Ju\,d\Omega=0 \tag{4.5}$$

Due to vector identity (A.14), taking $\varphi = u$ and $\overline{V}=\mu^{-1}\overline{\nabla}A$, it follows

$$\int_\Omega \overline{\nabla}\cdot\left(u\mu^{-1}\overline{\nabla}A\right)d\Omega-\int_\Omega \overline{\nabla}u\cdot\mu^{-1}\overline{\nabla}A\,d\Omega+\int_\Omega Ju\,d\Omega=0 \tag{4.6}$$

By applying Gauss's theorem one obtains

$$\begin{aligned}\int_\Gamma u\mu^{-1}\overline{\nabla}A\cdot\overline{n}\,d\Gamma-\int_\Omega\overline{\nabla}u\cdot\mu^{-1}\overline{\nabla}A\,d\Omega+\int_\Omega Ju\,d\Omega=\\ =\int_{\Gamma_D}u\mu^{-1}\overline{\nabla}A\cdot\overline{n}\,d\Gamma+\int_{\Gamma_N}u\mu^{-1}\frac{\partial A}{\partial n}d\Gamma+\\ -\int_\Omega\overline{\nabla}u\cdot\mu^{-1}\overline{\nabla}A\,d\Omega+\int_\Omega Ju\,d\Omega=0\end{aligned}\tag{4.7}$$

Due to boundary conditions (4.2) and (4.3) the first two terms are zero; therefore, it results

$$-\int_\Omega\overline{\nabla}u\cdot\mu^{-1}\overline{\nabla}A\,d\Omega+\int_\Omega Ju\,d\Omega=0\tag{4.8}$$

which is the variational equation associated to the differential equation (4.1).

Now, taking $u=\delta A$ where δA is the elementary variation of A, (4.8) becomes

$$-\int_\Omega\delta\overline{\nabla}A\cdot\mu^{-1}\overline{\nabla}A\,d\Omega+\int_\Omega J\delta A\,d\Omega=0\tag{4.9}$$

or, equivalently

$$\delta\left[\int_\Omega\left(\frac{1}{2\mu}\overline{\nabla}A\cdot\overline{\nabla}A-JA\right)d\Omega\right]=0\tag{4.10}$$

which states the necessary condition for A to be a steady point of the functional

$$\chi(A)=\int_\Omega\frac{1}{2\mu}\overline{\nabla}A\cdot\overline{\nabla}A\,d\Omega-\int_\Omega JA\,d\Omega\tag{4.11}$$

In other words, if A is a solution of differential equation (4.1) subject to (4.2) and (4.3), then A is a solution also of variational equation (4.10) and is such to give origin to a steady point of functional (4.11).

Conversely, having defined the energy functional of the simply connected domain Ω as

$$\chi=\int_\Omega\frac{1}{2\mu}\overline{\nabla}A\cdot\overline{\nabla}A\,d\Omega-\int_\Omega JA\,d\Omega\tag{4.12}$$

or, thanks to (2.15)

$$\chi=\int_\Omega\frac{1}{2\mu}\overline{B}\cdot\overline{B}\,d\Omega-\int_\Omega JA\,d\Omega\tag{4.13}$$

where

$$\overline{B}=\left(\frac{\partial A}{\partial y},-\frac{\partial A}{\partial x},0\right)=\left(\overline{\nabla}A\right)^\perp\tag{4.14}$$

(see Section 2.3.2), equation (4.1) follows.

In fact, let the first-order variation $\delta\chi$ of functional χ, which represents minus the co-energy of the domain Ω for given current density (see Section 2.3.5), be considered. It results

$$\begin{aligned}\delta\chi &= \int_\Omega \frac{1}{2\mu}\delta(\overline{\nabla}A\cdot\overline{\nabla}A)d\Omega - \int_\Omega J\delta A\, d\Omega = \\ &= \int_\Omega \left[\frac{1}{2\mu}\overline{\nabla}(\delta A)\cdot\overline{\nabla}A + \frac{1}{2\mu}\overline{\nabla}A\cdot\overline{\nabla}(\delta A)\right]d\Omega - \int_\Omega J\delta A\, d\Omega = \\ &= \int_\Omega \mu^{-1}\overline{\nabla}A\cdot\overline{\nabla}(\delta A)d\Omega - \int_\Omega J\delta A\, d\Omega\end{aligned} \tag{4.15}$$

Due to (A.14) with $\varphi = \delta A$ and $\overline{\nabla} = \mu^{-1}\overline{\nabla}A$ one has

$$\delta\chi = \int_\Omega \overline{\nabla}\cdot\left(\delta A\mu^{-1}\overline{\nabla}A\right)d\Omega - \int_\Omega \delta A\overline{\nabla}\cdot\left(\mu^{-1}\overline{\nabla}A\right)d\Omega - \int_\Omega J\delta A\, d\Omega \tag{4.16}$$

Then, applying Gauss's theorem, it follows

$$\begin{aligned}\delta\chi &= \int_\Gamma \delta A\mu^{-1}\overline{\nabla}A\cdot\overline{n}\, d\Gamma - \int_\Omega \delta A\big(\overline{\nabla}\cdot\mu^{-1}\overline{\nabla}A + J\big)d\Omega = \\ &= \int_{\Gamma_D} \mu^{-1}\delta A\overline{\nabla}A\cdot\overline{n}\, d\Gamma + \int_{\Gamma_N} \mu^{-1}\delta A\frac{\partial A}{\partial n}d\Gamma - \int_\Omega \delta A\big(\overline{\nabla}\cdot\mu^{-1}\overline{\nabla}A + J\big)d\Omega\end{aligned} \tag{4.17}$$

If A fulfils (4.2) and (4.3), one has

$$\delta\chi = -\int_\Omega \delta A\big(\overline{\nabla}\cdot\mu^{-1}\overline{\nabla}A + J\big)d\Omega \tag{4.18}$$

Since the co-energy has a steady point when $\delta\chi = 0$, the Poisson's equation

$$\overline{\nabla}\cdot\mu^{-1}\overline{\nabla}A + J = 0 \tag{4.19}$$

is verified; (4.19) is called the Euler's equation associated to functional (4.12)

As a result, the equivalence between the search of a solution to Poisson's equation and the search of a steady point of an energy functional has been proven. The two approaches are known as Ritz's method and Galerkin's method, respectively.

According to the latter, a numerical procedure approximating the minimization of the energy functional is developed.

The following remarks are applicable:

(i) Dirichlet's condition (4.2) is an essential boundary condition, because the value of A must be forced at least in a point of the boundary.
(ii) Homogeneous Neumann's condition (4.3) is a natural boundary condition, because it is already taken into account both in (4.7) and (4.17).

4.2 Finite Elements for Two-Dimensional Magnetostatics

4.2.1 Discretization of Energy Functional

Let the following continuous problem be considered: find the steady point of $\chi(A)$, $A = \text{const. along } \Gamma_D$, $\frac{\partial A}{\partial n} = 0$ along Γ_N, where

$$\chi(A) = \int_\Omega \frac{1}{2\mu}\left[\left(\frac{\partial A}{\partial x}\right)^2 + \left(\frac{\partial A}{\partial y}\right)^2\right] d\Omega - \int_\Omega JA\, d\Omega \tag{4.20}$$

is the energy functional associated to a simply-connected domain Ω in which rectangular coordinates are assumed. In (4.20) it is supposed that A is continuous up to its first derivative, while J is assumed to be a continuous function.

Let Ω be discretized by means of a grid of triangular elements subject to the following constraints (Fig. 4.1):

- Two adjacent elements do not overlap
- No vertex of a triangle belongs to the edge of an adjacent triangle

The following discretization of problem (4.20) is introduced: find the steady point of $\chi(A)$ for the net of triangles of the grid, upon the condition that the restriction of potential A to an element of the given grid is represented by a linear polynomial and $A = \text{const along } \Gamma_D$, $\frac{\partial A}{\partial n} = 0$ along Γ_N. As a consequence, in the whole domain the potential A is approximated by a piecewise-linear function.

Given a numbering of grid nodes ($i = 1, 2, \ldots, n$), the piecewise-linear functions

$$\begin{aligned} &\psi_i(x, y) = 1 \text{ at node } i = 1, n \\ &\psi_j(x, y) = 0 \text{ at all the other nodes } j = 1, n,\ j \neq i \end{aligned} \tag{4.21}$$

are called global shape functions (Fig. 4.2). A can be written as

$$A(x, y) = \sum_{i=1}^{n} \psi_i(x, y) A_i \tag{4.22}$$

where A_i is the unknown value of A(x, y) at ith node and A(x, y) varies linearly.

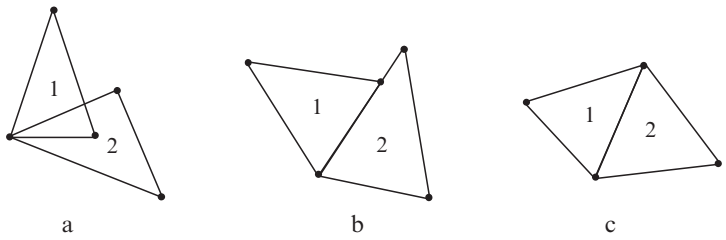

Fig. 4.1 Examples of incorrectly (**a, b**) and correctly (**c**) shaped triangles

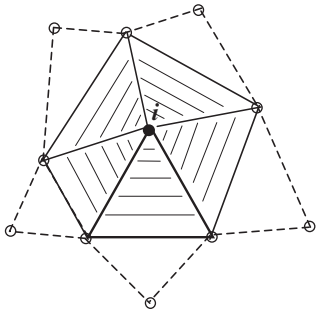

Fig. 4.2 Detail of a grid: representation of the global shape function associated to ith node. Shaded triangles show the linear variation of the function

After substituting (4.22) in (4.20) one obtains

$$\chi(A_1, A_2, \ldots, A_n) = \int_\Omega \frac{1}{2\mu}\left[\left(\sum_{i=1}^{n} A_i \frac{\partial \psi_i}{\partial x}\right)^2 + \left(\sum_{i=1}^{n} A_i \frac{\partial \psi_i}{\partial y}\right)^2\right] d\Omega + - \int_\Omega J \sum_{i=1}^{n} A_i \psi_i d\Omega \tag{4.23}$$

that represents the discrete version of (4.20).

In (4.23) the terms dependent on just A_i can be separated from those independent of A_i. Explicitly, one gets

$$\begin{aligned}\chi(A_1, A_2, \ldots, A_n) = {} & A_i^2 \int_\Omega \frac{1}{2\mu}\left[\left(\frac{\partial \psi_i}{\partial x}\right)^2 + \left(\frac{\partial \psi_i}{\partial y}\right)^2\right] d\Omega + \\ & + 2A_i \sum_{\substack{j=1 \\ j\neq i}}^{n} A_j \int_\Omega \frac{1}{2\mu}\left(\frac{\partial \psi_i}{\partial x}\frac{\partial \psi_j}{\partial x} + \frac{\partial \psi_i}{\partial y}\frac{\partial \psi_j}{\partial y}\right) d\Omega + \\ & - A_i \int_\Omega J\psi_i d\Omega - \sum_{\substack{k=1 \\ k\neq i}}^{n} A_k \int_\Omega J\psi_k d\Omega \end{aligned} \tag{4.24}$$

In order $A = (A_1,\ A_2, \ldots,\ A_n)$ to make functional (4.23) steady, it must be

$$\frac{\partial \chi}{\partial A_i} = 0, \quad i = 1, 2, \ldots, n \tag{4.25}$$

From (4.24) and (4.25) one obtains

$$\begin{aligned} & A_i \int_\Omega \mu^{-1} \left[\left(\frac{\partial \psi_i}{\partial x} \right)^2 + \left(\frac{\partial \psi_i}{\partial y} \right)^2 \right] d\Omega + \\ & + \sum_{\substack{j=1 \\ j \neq i}}^{n} A_j \int_\Omega \mu^{-1} \left(\frac{\partial \psi_i}{\partial x} \frac{\partial \psi_j}{\partial x} + \frac{\partial \psi_i}{\partial y} \frac{\partial \psi_j}{\partial y} \right) d\Omega + \\ & - \int_\Omega J \psi_i d\Omega = 0, \quad i = 1, 2, \ldots, n \end{aligned} \tag{4.26}$$

If should be noted that (4.26) represents a linear system of n equations in n unknowns A_i. If the system is expressed in matrix form, the entries of the coefficient matrix H(n, n) become

$$h_{ij} = \int_\Omega \frac{1}{\mu} \left(\frac{\partial \psi_i}{\partial x} \frac{\partial \psi_j}{\partial x} + \frac{\partial \psi_i}{\partial y} \frac{\partial \psi_j}{\partial y} \right) d\Omega, \quad i, j = 1, 2, \ldots, n \tag{4.27}$$

while the entries of the source vector d(n, 1) are

$$d_i = \int_\Omega J \psi_i \, d\Omega, \quad i = 1, 2, \ldots, n \tag{4.28}$$

Then, system (4.26) can be written in matrix form as

$$H \, A = d \tag{4.29}$$

where H(n, n) is the reluctance (H^{-1} m) matrix, while A(n, 1) and d(n, 1) are nodal potential (Wb m^{-1}) and nodal current (A) vectors, respectively.

It is easy to realize that in (4.27) functions ψ_i, ψ_j can be interchanged, i.e. matrix H is symmetric. The problem of finding a steady point of functional (4.23) is then reduced to the solution of a linear system governed by matrix H and source term d.

It should be noted that system (4.29) is singular; in order its solution to be unique, it is necessary to fix the value of potential A of all n_D nodes where (4.2) holds; at least one node located along boundary Γ must be constrained.

4.2.2 Local Shape Functions in Rectangular Coordinates

Referring to a triangle of the grid, the following local shape functions

$$\begin{aligned} & \psi_k(x, y) = 1 \ \text{ at node } k = 1, 2, 3 \text{ anticlockwise} \\ & \psi_k(x, y) = 0 \ \text{ at the other two nodes} \end{aligned} \tag{4.30}$$

with linear variation with respect to (x, y) can be introduced; they represent the restriction of (4.21) to node k of the triangle.

Referring to a triangle of vertices $V_1 = (x_1,\ y_1)$, $V_2 = (x_2,\ y_2)$, $V_3 = (x_3,\ y_3)$, the following functions

$$\begin{aligned}
\psi_1(x, y) &= \frac{1}{2S}\left[(x_2y_3 - x_3y_2) + x(y_2 - y_3) + y(x_3 - x_2)\right] \\
\psi_2(x, y) &= \frac{1}{2S}\left[(x_3y_1 - x_1y_3) + x(y_3 - y_1) + y(x_1 - x_3)\right] \\
\psi_3(x, y) &= \frac{1}{2S}\left[(x_1y_2 - x_2y_1) + x(y_1 - y_2) + y(x_2 - x_1)\right]
\end{aligned} \tag{4.31}$$

where

$$S = \frac{1}{2}\begin{vmatrix} 1 & x_1 & y_1 \\ 1 & x_2 & y_2 \\ 1 & x_3 & y_3 \end{vmatrix} \tag{4.32}$$

is the area of the triangle considered, are linear in both x and y. They fulfil conditions (4.30) and are the local shape functions. A geometric interpretation of (4.31) is given in Fig. 4.3.

Considering an inner point V(x, y), the ratio

$$\frac{s}{h} = \frac{S_1}{S_1 + S_2 + S_3} = \frac{S_1}{S} \tag{4.33}$$

is called area coordinate ξ_1 referred to vertex 1; in general, area coordinates are defined as

$$\xi_k = \frac{S_k}{S}, \quad k = 1, 2, 3 \tag{4.34}$$

The following properties hold

$$0 \le \xi_k \le 1,\ \sum_{k=1}^{3} \xi_k = 1, \quad k = 1, 2, 3 \tag{4.35}$$

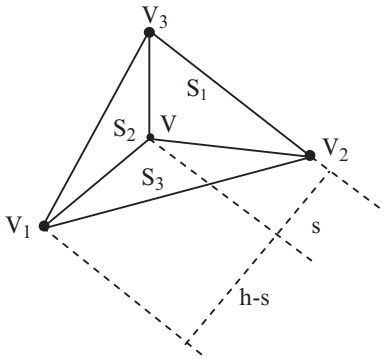

Fig. 4.3 Geometric interpretation of local shape functions

It can be proven that

$$\psi_k = \xi_k, \quad k = 1, 2, 3 \tag{4.36}$$

In fact, S_k is obtained by substituting vector [1 x, y] in the kth row of area matrix determinant (4.32); considering (4.34) and (4.31), (4.36) immediately follows.

Consequently, the restriction of potential A(x, y) to the given triangle is

$$A(x, y) = \sum_{k=1}^{3} \psi_k(x, y) A_k = \begin{bmatrix} \psi_1(x, y) & \psi_2(x, y) & \psi_3(x, y) \end{bmatrix} \begin{bmatrix} A_1 \\ A_2 \\ A_3 \end{bmatrix} \tag{4.37}$$

where A_1, A_2, A_3 are the nodal values of potential in the triangle itself.

4.2.3 Coefficient Matrix and Source Vector

If (4.27) is applied to all the triangular elements composing the grid, the entry h_{ij} is the sum of the contributions of each element e

$$h_{ij} = \sum \int_e \mu^{-1} \left(\frac{\partial \psi_i}{\partial x} \frac{\partial \psi_j}{\partial x} + \frac{\partial \psi_i}{\partial y} \frac{\partial \psi_j}{\partial y} \right) dx\, dy, \quad i, j = 1, 2, \ldots, n \tag{4.38}$$

where ψ_i, ψ_j are the global shape functions.

However, it is easily seen that the contribution of a triangle e to the integral in (4.38) is zero if either the ith or the jth node does not belong to triangle e itself. As a consequence, the majority of terms forming the integral is zero and the matrix is sparse.

In this respect, it is convenient to define the local coefficient matrix $H_e(3, 3)$ associated to a single triangle e having area S_e with entries

$$h_{k\lambda} = \int_e \mu^{-1} \left(\frac{\partial \psi_k}{\partial x} \frac{\partial \psi_\lambda}{\partial x} + \frac{\partial \psi_k}{\partial y} \frac{\partial \psi_\lambda}{\partial y} \right) dx\, dy, \quad k, \lambda = 1, 2, 3 \tag{4.39}$$

where ψ_k, ψ_λ are local shape functions.

From (4.31), by a cyclic permutation of indices, it results

$$\begin{aligned} \frac{\partial \psi_k}{\partial x} &= \frac{y_{k+1} - y_{k+2}}{2S_e} \equiv \frac{a_k}{2S_e} \\ \frac{\partial \psi_k}{\partial y} &= \frac{x_{k+2} - x_{k+1}}{2S_e} \equiv \frac{b_k}{2S_e} \end{aligned} \tag{4.40}$$

with k = 1, 2, 3 and $x_4 = x_1$, $x_5 = x_2$, $y_4 = y_1$, $y_5 = y_2$. The entries of the local coefficient matrix (4.39) are then given by

$$h_{k\lambda} = \int_e \left(\frac{a_k a_\lambda + b_k b_\lambda}{4\mu S_e^2} \right) dx\, dy = \frac{a_k a_\lambda + b_k b_\lambda}{4\mu S_e}, \quad k, \lambda = 1, 2, 3 \tag{4.41}$$

In practice, the entries of the global matrix are assembled starting from entries of local matrices, for the correspondence between local and global numbering of nodes is unique. The assembling rules will be clarified later on by means of an example.

In a similar way, it is possible to construct (4.28) by assembling local contributions; in fact

$$d_i = \int_\Omega J\psi_i d\Omega = \sum \int_e J\psi_k \, dx \, dy, \quad i = 1, 2, \ldots, n, \quad k = 1, 2, 3 \tag{4.42}$$

The local source vector d_e associated to a single triangle e has entry

$$d_k = \int_e J\psi_k \, dx \, dy, \quad k = 1, 2, 3 \tag{4.43}$$

In particular, if current density J is assumed to be constant in the element considered, each local source term is equal to $\frac{JS_e}{3}$.

4.2.4 From Potential to Field

Assuming that the magnetic potential A (x, y) is approximated by a linear polynomial on each element of the grid, if A_1, A_2, A_3 are the values of potential in vertices $V_1 = (x_1, y_1)$, $V_2 = (x_2, y_2)$, $V_3 = (x_3, y_3)$ of triangle e, respectively, the induction field $\overline{B} = (B_x, B_y, B_z)$ is approximated on each element by

$$\overline{B} = \left(\frac{\partial A}{\partial y}, -\frac{\partial A}{\partial x}, 0 \right) \tag{4.44}$$

From (4.32) and (4.37) it results

$$\begin{bmatrix} B_x \\ B_y \end{bmatrix} = \frac{1}{2S_e} \begin{bmatrix} x_3 - x_2 & x_1 - x_3 & x_2 - x_1 \\ y_3 - y_2 & y_1 - y_3 & y_2 - y_1 \end{bmatrix} \begin{bmatrix} A_1 \\ A_2 \\ A_3 \end{bmatrix} = \tag{4.45}$$

$$= \frac{1}{2S_e} \begin{bmatrix} b_1 & b_2 & b_3 \\ -a_1 & -a_2 & -a_3 \end{bmatrix} \begin{bmatrix} A_1 \\ A_2 \\ A_3 \end{bmatrix}$$

Apparently, matrix

$$\frac{1}{2S_e} \begin{bmatrix} b_1 & b_2 & b_3 \\ -a_1 & -a_2 & -a_3 \end{bmatrix} \tag{4.46}$$

approximates the curl operator.

The following remark can be put forward. At the interface between two triangles, having an edge in common, both normal component B_n of induction field and tangential component of magnetic field $H_t = \mu^{-1} B_t$ are not continuous. In other words, field components are approximated by means of piecewise constant functions all over the domain.

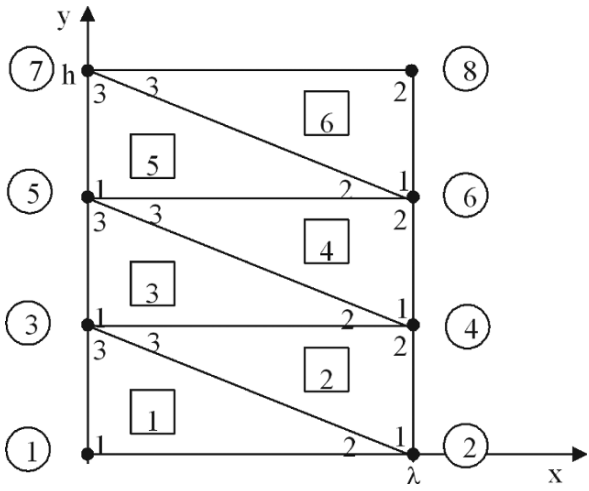

Fig. 4.4 Grid discretizing a half-slot

4.2.5 Magnetic Field in a Slot Solved by the Finite Element Method

Let the test problem shown in Fig. 2.13a be considered. The rectangular domain corresponding to half a slot is discretized by means of six triangular elements numbered, for instance, as shown in Fig. 4.4. The n nodes are numbered from 1 to 8 arbitrarily within the grid and from 1 to 3 (anticlockwise) inside each triangle.

According to (4.41), the coefficient matrix associated to a triangle e having vertices $V_1 = (x_1,\ y_1),\ V_2 = (x_2,\ y_2)$ and $V_3 = (x_3,\ y_3)$ results

$$H_e = \frac{1}{4\mu S}\begin{bmatrix} (y_2-y_3)^2+ & (y_2-y_3)(y_3-y_1)+ & (y_2-y_3)(y_1-y_2)+ \\ +(x_3-x_2)^2 & +(x_3-x_2)(x_1-x_3) & +(x_3-x_2)(x_2-x_1) \\ & & \\ & (y_3-y_1)^2+ & (y_3-y_1)(y_1-y_2)+ \\ & +(x_1-x_3)^2 & +(x_1-x_3)(x_2-x_1) \\ & & \\ \text{symmetric} & & (y_1-y_2)^2+ \\ & & +(x_2-x_1)^2 \end{bmatrix} \tag{4.47}$$

where μ and S are magnetic permeability and area of the triangle, respectively.

For element 1, given height h and half-width λ of the slot, one has $V_1 = (0,\ 0),\ V_2 = (\lambda,\ 0),\ V_3 = (0,\ \frac{h}{3})$ and the local coefficient matrix is:

$$H_1 = \frac{1}{4\mu S}\begin{bmatrix} \frac{h^2}{9}+\lambda^2 & -\frac{h^2}{9} & -\lambda^2 \\ & \frac{h^2}{9} & 0 \\ \text{symm.} & & \lambda^2 \end{bmatrix} \tag{4.48}$$

Analogously, for element 2, one has $V_1 = (\lambda,\ 0),\ V_2 = (\lambda,\ \frac{h}{3}),\ V_3 = (0,\ \frac{h}{3})$ and the local coefficient matrix is:

$$H_2 = \frac{1}{4\mu S}\begin{bmatrix} \lambda^2 & -\lambda^2 & 0 \\ & \frac{h^2}{9}+\lambda^2 & -\frac{h^2}{9} \\ \text{symm.} & & \frac{h^2}{9} \end{bmatrix} \tag{4.49}$$

From Fig. 4.4 it can be noted that elements 3 and 5 correspond to element 1 and keep the same local numbering of nodes as in element 1. The same happens for elements 4 and 6 with respect to element 2. Therefore, it results: $H_3 = H_1$ and $H_5 = H_1;\ H_4 = H_2$ and $H_6 = H_2$.

Supposing current density J is uniform, local source terms are all equal to $\frac{JS}{3}$ in each triangle and

$$d_e = \frac{JS}{3}\begin{bmatrix} 1 \\ 1 \\ 1 \end{bmatrix} \tag{4.50}$$

In general, the global coefficient matrix H can be assembled node by node according to the following rule:

- Diagonal terms h_{ii} are obtained as the sum of the corresponding terms of local matrices of all triangles having ith node in common
- Off-diagonal terms h_{ij} are obtained by summing the corresponding terms of local matrices of the two triangles sharing the edge between ith node and jth node

For instance, global node 1 belongs to element 1 only, corresponding to local node 1; therefore $H(1,\ 1) = H_1(1,\ 1)$. Moreover, global node 2 is in common between elements 1 and 2 for which it corresponds to local nodes 2 and 1, respectively; therefore $H(2,\ 2) = H_1(2,\ 2) + H_2(1,\ 1)$. Going on, global node 3 is in common among elements 1, 2, 3 where it corresponds to local nodes 3, 3, 1 respectively; therefore $H(3,\ 3) = H_1(3,\ 3) + H_2(3,\ 3) + H_3(1,\ 1)$.

Passing to off-diagonal terms, for the sake of an example, the edge joining global node 3 to global node 4 is in common between elements 2 and 3; moreover, global node 4 corresponds to local node 2 in both elements 2 and 3; therefore one has $H(3,\ 4) = H_2(2,\ 3) + H_3(1,\ 2) = H(4,\ 3)$.

By iterating the assembling algorithm on all global nodes, finally it results:

$$H = \frac{1}{4\mu S}\begin{bmatrix} \frac{h^2}{9}+\lambda^2 & -\frac{h^2}{9} & -\lambda^2 & 0 & 0 & 0 & 0 & 0 \\ & \frac{h^2}{9}+\lambda^2 & 0 & -\lambda^2 & 0 & 0 & 0 & 0 \\ & & 2\frac{h^2}{9}+2\lambda^2 & -2\frac{h^2}{9} & -\lambda^2 & 0 & 0 & 0 \\ & & & 2\frac{h^2}{9}+2\lambda^2 & 0 & -\lambda^2 & 0 & 0 \\ & & & & 2\frac{h^2}{9}+2\lambda^2 & -2\frac{h^2}{9} & -\lambda^2 & 0 \\ & & & & & 2\frac{h^2}{9}+2\lambda^2 & 0 & -\lambda^2 \\ & \text{symmetric} & & & & & \frac{h^2}{9}+\lambda^2 & -\frac{h^2}{9} \\ & & & & & & & \frac{h^2}{9}+\lambda^2 \end{bmatrix} \tag{4.51}$$

It can be noted that H is sparse and has a bandwidth that depends on the global numbering of the grid nodes; moreover, it exhibits diagonal-dominance, in fact $H(i,i) \geq \sum_{j=i+1}^{n} |H(i,j)|,\ i = 1,\ n-1$. By assembling local contributions node by node, the source vector d(n, 1) is obtained:

$$d = \frac{JS}{3}[1\,2\,3\,3\,3\,3\,2\,1]^T \tag{4.52}$$

In this way, the solving system (4.29) results.

In order matrix H(n, n) to be non-singular, the boundary condition of Dirichlet's type should be imposed in at least one node. In the test problem: $A_1 = A_2 = 0$. In order to fulfil $A_1 = 0$, the first row and the first column of H are cancelled, while to fulfil $A_2 = 0$ the second row and the second column of H are cancelled, so obtaining a matrix $H'(n-2,\ n-2)$ that is non-singular. Correspondingly, the first and the second terms of source vector are cancelled, obtaining a vector $d'(n-2,\ 1)$. Finally, the reduced algebraic system comes out

$$H'A' = d' \tag{4.53}$$

with

$$H' = \frac{1}{4\mu S}\begin{bmatrix} 2\frac{h^2}{9}+2\lambda^2 & -2\frac{h^2}{9} & -\lambda^2 & 0 & 0 & 0 \\ & 2\frac{h^2}{9}+2\lambda^2 & 0 & -\lambda^2 & 0 & 0 \\ & & 2\frac{h^2}{9}+2\lambda^2 & -2\frac{h^2}{9} & -\lambda^2 & 0 \\ & & & 2\frac{h^2}{9}+2\lambda^2 & 0 & -\lambda^2 \\ & \text{symmetric} & & & \frac{h^2}{9}+\lambda^2 & -\frac{h^2}{9} \\ & & & & & \frac{h^2}{9}+\lambda^2 \end{bmatrix} \tag{4.54}$$

and

$$d' = \frac{JS}{3}[3\,3\,3\,3\,2\,1]^T \tag{4.55}$$

It should be noted that matrix H′ is better conditioned than matrix H owing to the specification of boundary condition of the Dirichlet's kind.

More generally, when the potential A_k to be imposed in the kth node is different from zero, one should proceed as follows:

- Set $H(k,j) = 0,\ \ j = 1,n,\ j \neq k$
- Set $H(i,k) = 0,\ \ i = 1,n,\ i \neq k$
- Leave H(k,k) unaltered
- Replace d_k with $H(k,k)A_k$
- Replace d_i with $d_i - H(i,k)A_k,\ \ i = 1,n,\ i \neq k.$

The sizes of matrix H and vector d remain unchanged.

A few physical remarks are worth being considered. The elements of system matrix, measured in $[H^{-1}m]$, depend on geometry and material property. In turn, the

source term JS, measured in [A], can be regarded as the current attributed to element e while $\frac{JS}{3}$ represents the nodal current.

From the numerical viewpoint, the following data are assumed: $h = 6\,cm,\ \lambda = 1\,cm,\ \mu = 1.25610^{-6}\ H\,m^{-1},\ J = 10^5\ A\,m^{-2}$.

All triangles have surface area $S = 1\,cm^2$. Considering these data, the condition number of H is $4.5594\ 10^{16}$, while that of H′ is 120. Matrix H′ is definite positive; therefore, the solution of the linear system is unique. The solution of the reduced system (4.54)–(4.55) is

$$\begin{bmatrix} A_3 \\ A_4 \\ A_5 \\ A_6 \\ A_7 \\ A_8 \end{bmatrix} = 10^{-3} \begin{bmatrix} 0.1256 \\ 0.1256 \\ 0.2010 \\ 0.2009 \\ 0.2270 \\ 0.2251 \end{bmatrix} \left(\frac{Wb}{m}\right) \tag{4.56}$$

Calculation of the induction field

Knowing node potentials, the components of induction field ($Wb\,m^{-2}$) can be obtained applying (4.45) element by element. To this end, the correspondence between local and global numbering of nodes, shown in Table 4.1, should be taken into account.

Element 1

$$\begin{bmatrix} B_x \\ B_y \end{bmatrix} = \frac{1}{2S} \begin{bmatrix} -\lambda & 0 & \lambda \\ \frac{h}{3} & -\frac{h}{3} & 0 \end{bmatrix} \begin{bmatrix} A_1 \\ A_2 \\ A_3 \end{bmatrix} = 10^{-3} \begin{bmatrix} -50 & 0 & 50 \\ 100 & -100 & 0 \end{bmatrix} \begin{bmatrix} 0 \\ 0 \\ 0.1256 \end{bmatrix}$$
$$= 10^{-3} \begin{bmatrix} 6.2801 \\ 0 \end{bmatrix}$$

Element 2

$$\begin{bmatrix} B_x \\ B_y \end{bmatrix} = \frac{1}{2S} \begin{bmatrix} -\lambda & \lambda & 0 \\ 0 & -\frac{h}{3} & \frac{h}{3} \end{bmatrix} \begin{bmatrix} A_2 \\ A_4 \\ A_3 \end{bmatrix} = 10^{-3} \begin{bmatrix} -50 & 50 & 0 \\ 0 & -100 & 100 \end{bmatrix} \begin{bmatrix} 0 \\ 0.1256 \\ 0.1256 \end{bmatrix}$$

Table 4.1 Correspondence between local and global nodes

Element	Local nodes	Global nodes
1	1, 2, 3	1, 2, 3
2	1, 2, 3	2, 4, 3
3	1, 2, 3	3, 4, 5
4	1, 2, 3	4, 6, 5
5	1, 2, 3	5, 6, 7
6	1, 2, 3	6, 8, 7

$$= 10^{-3} \begin{bmatrix} 6.2799 \\ 0 \end{bmatrix}$$

Element 3

$$\begin{bmatrix} B_x \\ B_y \end{bmatrix} = \frac{1}{2S} \begin{bmatrix} -\lambda & 0 & \lambda \\ \frac{h}{3} & -\frac{h}{3} & 0 \end{bmatrix} \begin{bmatrix} A_3 \\ A_4 \\ A_5 \end{bmatrix} = 10^{-3} \begin{bmatrix} -50 & 0 & 50 \\ 100 & -100 & 0 \end{bmatrix} \begin{bmatrix} 0.1256 \\ 0.1256 \\ 0.2010 \end{bmatrix}$$
$$= 10^{-3} \begin{bmatrix} 3.7705 \\ 0 \end{bmatrix}$$

Element 4

$$\begin{bmatrix} B_x \\ B_y \end{bmatrix} = \frac{1}{2S} \begin{bmatrix} -\lambda & \lambda & 0 \\ 0 & -\frac{h}{3} & \frac{h}{3} \end{bmatrix} \begin{bmatrix} A_4 \\ A_6 \\ A_5 \end{bmatrix} = 10^{-3} \begin{bmatrix} -50 & 50 & 0 \\ 0 & -100 & 100 \end{bmatrix} \begin{bmatrix} 0.1256 \\ 0.2009 \\ 0.2010 \end{bmatrix}$$
$$= 10^{-3} \begin{bmatrix} 3.7655 \\ 1.043410^{-2} \end{bmatrix}$$

Element 5

$$\begin{bmatrix} B_x \\ B_y \end{bmatrix} = \frac{1}{2S} \begin{bmatrix} -\lambda & 0 & \lambda \\ \frac{h}{3} & -\frac{h}{3} & 0 \end{bmatrix} \begin{bmatrix} A_5 \\ A_6 \\ A_7 \end{bmatrix} = 10^{-3} \begin{bmatrix} -50 & 0 & 50 \\ 100 & -100 & 0 \end{bmatrix} \begin{bmatrix} 0.2010 \\ 0.2009 \\ 0.2270 \end{bmatrix}$$
$$= 10^{-3} \begin{bmatrix} 1.3002 \\ 1.043410^{-2} \end{bmatrix}$$

Element 6

$$\begin{bmatrix} B_x \\ B_y \end{bmatrix} = \frac{1}{2S} \begin{bmatrix} -\lambda & \lambda & 0 \\ 0 & -\frac{h}{3} & \frac{h}{3} \end{bmatrix} \begin{bmatrix} A_6 \\ A_8 \\ A_7 \end{bmatrix} = 10^{-3} \begin{bmatrix} -50 & 50 & 0 \\ 0 & -100 & 100 \end{bmatrix} \begin{bmatrix} 0.2009 \\ 0.2251 \\ 0.2270 \end{bmatrix}$$
$$= 10^{-3} \begin{bmatrix} 1.2118 \\ 1.872310^{-1} \end{bmatrix}$$

Finally, it results

$$\begin{bmatrix} B_{1x} \\ B_{2x} \\ B_{3x} \\ B_{4x} \\ B_{5x} \\ B_{6x} \end{bmatrix} = 10^{-3} \begin{bmatrix} 6.2801 \\ 6.2799 \\ 3.7705 \\ 3.7655 \\ 1.3002 \\ 1.2118 \end{bmatrix}; \begin{bmatrix} B_{1y} \\ B_{2y} \\ B_{3y} \\ B_{4y} \\ B_{5y} \\ B_{6y} \end{bmatrix} = 10^{-6} \begin{bmatrix} 0 \\ 0 \\ 0 \\ 10.434 \\ 10.434 \\ 187.23 \end{bmatrix} \tag{4.57}$$

It should be remarked that in odd elements the value of B_y depends on $A_1 - A_2$ and symmetry implies $A_1 = A_2$ (indexes 1 and 2 refer to the local numbering); in an analogous way, in even elements the value of B_y depends on $-A_2 + A_3$ and symmetry implies $A_2 = A_3$ (indexes 2 and 3 refer to the local numbering). Residuals of B_y are due to approximation error in computing potentials.

Table 4.2 Distribution of nodal error (Fig. 4.4)

Node	3	4	5	6	7	8
Y coordinate	0.02		0.04		0.06	
E_i	-2.3076 10^{-5}	2.3076 10^{-5}	-2.5961 10^{-4}	2.5961 10^{-4}	-4.1409 10^{-3}	4.1409 10^{-3}

Error analysis

The test problem has an exact analytical solution, namely

$$A = \mu J \left(hy - \frac{1}{2} y^2 \right) \tag{4.58}$$

$$\left(B_x, B_y \right) = \left(\mu J \left(h - y \right), 0 \right) \tag{4.59}$$

such that $A = 0$ at $y = 0$ and $0 < y < h$.

As far as potential is concerned, the local error

$$E_i = 1 - \frac{A(i)}{A_i}, \quad i = 3, 8 \tag{4.60}$$

can be defined, where $A(i)$ and A_i are approximated and exact values of potential at the ith node, respectively. The distribution of error is reported in Table 4.2.

It can be noted that the local error increases with the distance from constrained nodes 1, 2; moreover, the potential is overestimated at the left-boundary nodes ($x = 0$) and underestimated at the right-boundary nodes ($x = \lambda$).

In order to test the effect of grid on accuracy, the following norms are introduced

$$\| f \|_2 = \sqrt{\sum_{i=3}^{n_p} [f(i)]^2} \tag{4.61}$$

and

$$\| f \|_\infty = \max_{i=3,n_p} \{ f(i) \} \tag{4.62}$$

with $n_p = 8$ grid nodes.

In terms of the residual it results

$$f(i) = \left| 1 - \frac{A_g(i)}{A_i} \right| \tag{4.63}$$

where A_g is the approximated value of potential computed using grid g while A_i is the exact one.

Having fixed the size of the slot, the test problem can be solved using grids with an increasing number of triangular elements.

Table 4.3 Error norms

No. of elements	6	30	46	330	1210
$\|f\|_2$	$0.286\ 10^{-2}$	$0.160\ 10^{-2}$	$0.441\ 10^{-3}$	$0.233\ 10^{-3}$	$0.140\ 10^{-3}$
$\|f\|_\infty$	$0.414\ 10^{-2}$	$0.200\ 10^{-2}$	$0.504\ 10^{-3}$	$0.252\ 10^{-3}$	$0.168\ 10^{-3}$

Table 4.4 Error on elements (coarsest grid)

Element	1	2	3	4	5	6
E_e	0.0624784	−0.0714038	0.0994116	−0.1242645	0.2236068	−0.4472136

The results obtained using different grids give rise to the error norms reported in Table 4.3; the latter decrease monotonically with the number of elements. In particular, $\|f\|_2$ and $\|f\|_\infty$ give a measurement of average and maximum error, respectively.

In turn, the error in terms of x component of induction field can be defined, in each element, as follows

$$E_e = 1 - \frac{B_e}{B} \tag{4.64}$$

where B_e and B are approximated and exact value of the x component of the induction field, respectively; the exact value is that referred to the gravity centre of the element. In Table 4.4 the distribution of error is reported, referring to the coarsest grid composed of six elements.

Again, it can be noted that the error increases as long as the distance from constrained nodes increases.

Finally, Fig. 4.5 shows the plot of flux lines. The results have been obtained using a grid composed of 736 triangles with linear variation of potential.

Remarks on the topology of the grid

From Table 4.2 it can be remarked that the approximated values of potential in the left boundary nodes are greater than the values of corresponding right boundary nodes. This discrepancy can be attributed to the grid asymmetry. In fact, let a new grid be considered, as the mirror-image with respect to the previous one; it is shown in Fig. 4.6.

The coefficient matrices of elements 1 and 2 are

$$H_1 = \frac{1}{4\mu S}\begin{bmatrix} \frac{h^2}{9} & -\frac{h^2}{9} & 0 \\ & \frac{h^2}{9}+\lambda^2 & -\lambda^2 \\ \text{symm.} & & \lambda^2 \end{bmatrix} \tag{4.65}$$

$$H_2 = \frac{1}{4\mu S}\begin{bmatrix} \lambda^2 & 0 & -\lambda^2 \\ & \frac{h^2}{9} & -\frac{h^2}{9} \\ \text{symm.} & & \frac{h^2}{9}+\lambda^2 \end{bmatrix} \tag{4.66}$$

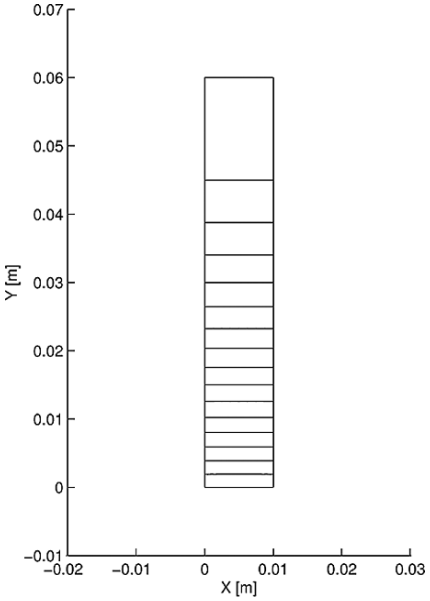

Fig. 4.5 Open slot: plot of flux lines

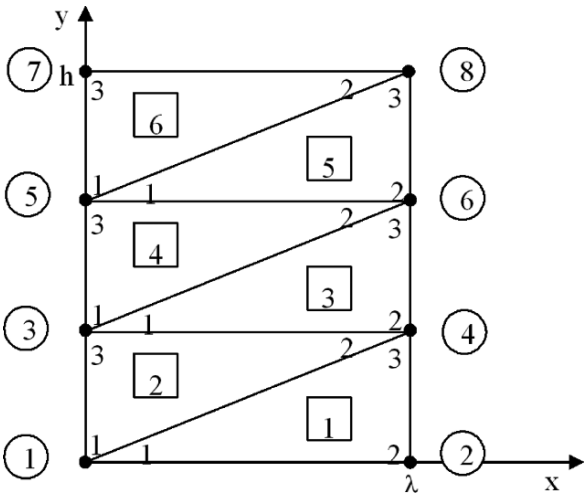

Fig. 4.6 Right-oriented grid discretizing half a slot

respectively. Keeping the same local numbering of nodes, one has $H_3 = H_1$ and $H_5 = H_1$; $H_4 = H_2$ and $H_6 = H_2$. In turn, local source terms are equal in all the elements

$$d_1 = d_2 = d_3 = d_4 = d_5 = d_6 = \frac{1}{3}JS \tag{4.67}$$

By assembling local coefficient matrices and source vectors the system

$$\mathrm{H}^{*}\mathrm{A}^{*} = \mathrm{d}^{*} \tag{4.68}$$

with

$$\mathrm{d}^{*} = \frac{\mathrm{JS}}{3}\,(2, 1, 3, 3, 3, 3, 1, 2)^{\mathrm{T}} \tag{4.69}$$

results. It can be remarked that H^{*} is the same as H in the previous case (4.51); in turn, d^{*} has first and second elements exchanged with respect to d, next-to-the-last and last elements exchanged as well, the other four components being unmodified.

After imposing boundary conditions in nodes 1 and 2 and introducing numerical data, the non-singular system

$$310^{5}\begin{bmatrix} 1.9904 & -1.5924 & -0.1990 & 0 & 0 & 0 \\ & 1.9904 & 0 & -0.1990 & 0 & 0 \\ & & 1.9904 & -1.5924 & -0.1990 & 0 \\ & & & 1.9904 & 0 & -0.1990 \\ & \text{symmetric} & & & 0.9952 & -0.7962 \\ & & & & & 0.9952 \end{bmatrix}\begin{bmatrix} \mathrm{A}_3 \\ \mathrm{A}_4 \\ \mathrm{A}_5 \\ \mathrm{A}_6 \\ \mathrm{A}_7 \\ \mathrm{A}_8 \end{bmatrix} = \begin{bmatrix} 3 \\ 3 \\ 3 \\ 3 \\ 1 \\ 2 \end{bmatrix} \tag{4.70}$$

is obtained, the solution of which is

$$\begin{bmatrix} \mathrm{A}_3 \\ \mathrm{A}_4 \\ \mathrm{A}_5 \\ \mathrm{A}_6 \\ \mathrm{A}_7 \\ \mathrm{A}_8 \end{bmatrix} = 10^{-3}\begin{bmatrix} 0.1255 \\ 0.1256 \\ 0.2009 \\ 0.2010 \\ 0.2251 \\ 0.2270 \end{bmatrix}\left(\frac{\mathrm{Wb}}{\mathrm{m}}\right) \tag{4.71}$$

The mirror-like aspect of the grid gives rise to the exchange of two pairs of components of the source vector.

As shown in Table 4.5, this exchange has the final effect of making the potentials at right-boundary nodes overestimated with respect to the corresponding potentials at left-boundary nodes.

Table 4.5 Distribution of nodal error (Fig. 4.6)

Node	3	4	5	6	7	8
Y coordinate	0.02		0.04		0.06	
$\mathrm{E_i}$	$3076\ 10^{-5}$	$-2.3076\ 10^{-5}$	$2.5961\ 10^{-4}$	$-2.5961\ 10^{-4}$	$4.1409\ 10^{-3}$	$-4.1409\ 10^{-3}$

4.3 Finite Elements for Three-Dimensional Magnetostatics

4.3.1 Surface and Solid Modelling

Generally, the three-dimensional model of an object can be built by means of either of two techniques: surface modelling and solid modelling, respectively.

According to the former, given a rectangular reference system, the orthogonal projection of the given object onto one of the three coordinate planes (Oxy, Oyz, Oxz) defines the base plane, which is then extruded to form volumes. Subsequently, the finite-element mesh is generated in two steps: first, a surface mesh is created in the base plane, using triangles or quadrilateral elements; next, the volume mesh follows, based on tetrahedrons or prisms, if the surface mesh is composed of triangles, or on hexahedral elements, otherwise.

In turn, solid modelling uses three-dimensional elementary volumes and Boolean operations to build the model of the object. This technique allows generating an object through operations such as transformations and combinations. Basic elements are parallelepipeds, cylinders, discs, spheres, cones, pyramids and thoroids; they can be generated at any point and then combined. Using Boolean operators, basic elements can also be merged, intersected or subtracted to model complex geometries. Finally, the finite-element mesh is generated, based on either tetrahedra or hexahedra or prismatic elements.

4.3.2 Local Shape Functions in Rectangular Coordinates

The extension of the results of Section 4.2 to the three-dimensional case can be easily obtained.

Let the domain Ω be discretised by means of a grid of tetrahedral elements, such that:

- Two adjacent elements do not overlap
- No vertex of a tetrahedron belongs to either the face or the edge of an adjacent tetrahedron

Moreover, let the magnetic potential be approximated by means of a linear polynomial within the element.

For the sake of simplicity, only the case of a source-free simply-connected field region is considered; consequently, the scalar magnetic potential $\phi(x, y, z)$ can be used (see 2.212).

Referring to a tetrahedron of vertices $v_i = (x_i, y_i, z_i)$ $i = 1, 4$, the following functions

$$\psi_i(x, y, z) = \frac{\det(C_i)}{\det(C)}, \quad i = 1, 4 \tag{4.72}$$

can be defined, where

$$\det(C) = \begin{vmatrix} 1 & x_1 & y_1 & z_1 \\ 1 & x_2 & y_2 & z_2 \\ 1 & x_3 & y_3 & z_3 \\ 1 & x_4 & y_4 & z_4 \end{vmatrix} = 6V \tag{4.73}$$

In (4.73) V is the volume of the given tetrahedron, det(C) is constant while

$$\det(C_1) = \begin{vmatrix} 1 & x & y & z \\ 1 & x_2 & y_2 & z_2 \\ 1 & x_3 & y_3 & z_3 \\ 1 & x_4 & y_4 & z_4 \end{vmatrix}, \quad \det(C_2) = \begin{vmatrix} 1 & x_1 & y_1 & z_1 \\ 1 & x & y & z \\ 1 & x_3 & y_3 & z_3 \\ 1 & x_4 & y_4 & z_4 \end{vmatrix}$$

$$\det(C_3) = \begin{vmatrix} 1 & x_1 & y_1 & z_1 \\ 1 & x_2 & y_2 & z_2 \\ 1 & x & y & z \\ 1 & x_4 & y_4 & z_4 \end{vmatrix}, \quad \det(C_4) = \begin{vmatrix} 1 & x_1 & y_1 & z_1 \\ 1 & x_2 & y_2 & z_2 \\ 1 & x_3 & y_3 & z_3 \\ 1 & x & y & z \end{vmatrix} \tag{4.74}$$

are linear functions of the coordinates (x, y, z) of a point P inside the tetrahedron.

A straightforward geometric interpretation in terms of volume coordinates is possible (Fig. 4.7); in fact, the denominator of (4.72) is proportional to the volume of the given tetrahedron, while the numerator is proportional to the volume of another tetrahedron, included into the given one and having the ith vertex coincident with point P(x, y, z).

It is easy to prove that $0 \leq \psi_k \leq 1$, $k = 1, 4$ and $\sum_{k=1}^{4} \psi_k(x, y, z) = 1$. Consequently, (4.72) can be assumed as the local shape functions.

In turn, the restriction of potential $\phi(x, y, z)$ to the tetrahedron is

$$\begin{aligned} \phi(x, y, z) &= \sum_{k=1}^{4} \psi_k(x, y, z)\phi_k \\ &= [\psi_1(x, y, z)\ \psi_2(x, y, z)\ \psi_3(x, y, z)\ \psi_4(x, y, z)] \begin{bmatrix} \phi_1 \\ \phi_2 \\ \phi_3 \\ \phi_4 \end{bmatrix} \end{aligned} \tag{4.75}$$

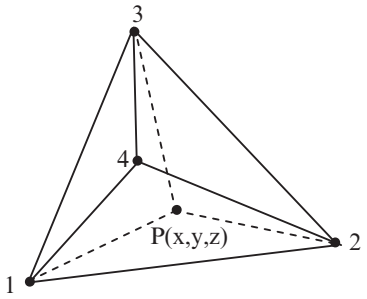

Fig. 4.7 Geometric interpretation of 3D local shape functions

where $(\phi_1,\ \phi_2,\ \phi_2,\ \phi_4)$ are the nodal values of the potential at the vertices $V_i = (x_i,\ y_i,\ z_i),\ i = 1,\ 4$ of tetrahedron.

The coefficient matrix and source vector are formed and assembled like in Sections 4.2.3 and 4.2.5, respectively.

A similar procedure applies when passing from the potential to the induction field $\overline{B} = \left(B_x,\ B_y,\ B_z\right)$ which is approximated on each element by

$$\overline{B} = -\mu\left(\frac{\partial\varphi}{\partial x}, \frac{\partial\varphi}{\partial y}, \frac{\partial\varphi}{\partial z}\right) \tag{4.76}$$

From (4.72) and (4.75) it follows

$$\begin{bmatrix} B_x \\ B_y \\ B_z \end{bmatrix} = -\mu \begin{bmatrix} \frac{\partial\psi_1}{\partial x} & \frac{\partial\psi_2}{\partial x} & \frac{\partial\psi_3}{\partial x} & \frac{\partial\psi_4}{\partial x} \\ \frac{\partial\psi_1}{\partial y} & \frac{\partial\psi_2}{\partial y} & \frac{\partial\psi_3}{\partial y} & \frac{\partial\psi_4}{\partial y} \\ \frac{\partial\psi_1}{\partial z} & \frac{\partial\psi_2}{\partial z} & \frac{\partial\psi_3}{\partial z} & \frac{\partial\psi_4}{\partial z} \end{bmatrix} \begin{bmatrix} \phi_1 \\ \phi_2 \\ \phi_3 \\ \phi_4 \end{bmatrix} \tag{4.77}$$

where μ is the element permeability.

Since (4.72) are linear in (x, y, z), each entry in the gradient matrix above is constant; therefore, the induction field in the domain Ω is approximated by means of a piecewise-constant function.

4.3.3 Comparison of 2D and 3D Simulations of an Electromagnet

Let the electromagnet discussed in Section 2.3.6 be considered again. The magnetic field is here computed by means of the finite-element method, based on both two-dimensional and three-dimensional models.

In Fig. 4.8 the two-dimensional mesh of the electromagnet is represented, for an air-gap $t = 1$ mm wide; the mesh is composed of 4,500 triangles, approximately. The resulting vector plot of the induction field is represented in Fig. 4.9; the air-gap

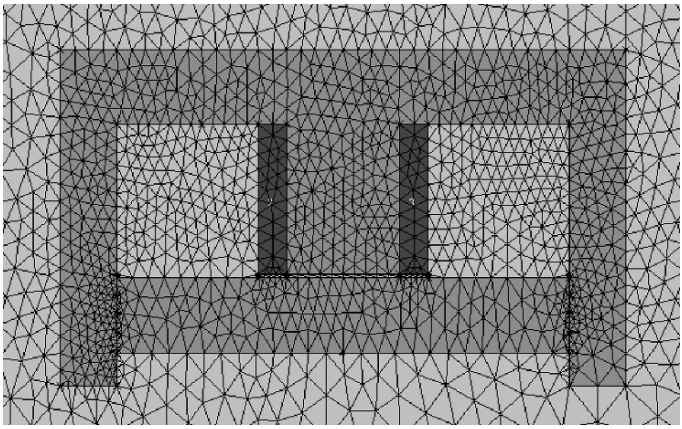

Fig. 4.8 2D finite-element mesh of the electromagnet ($t = 1$ mm)

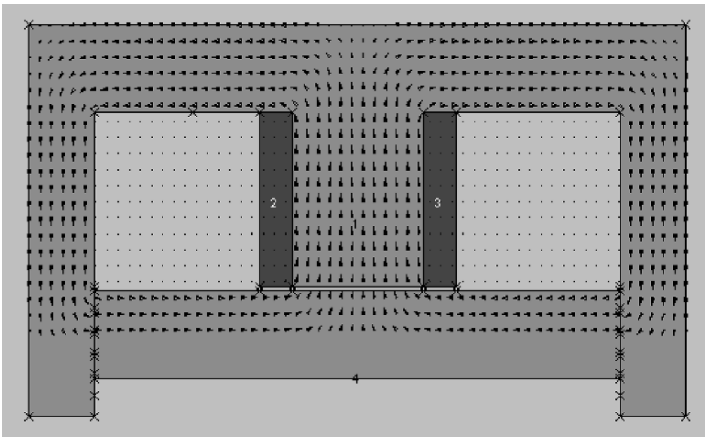

Fig. 4.9 Vector plot of magnetic induction (t = 1 mm)

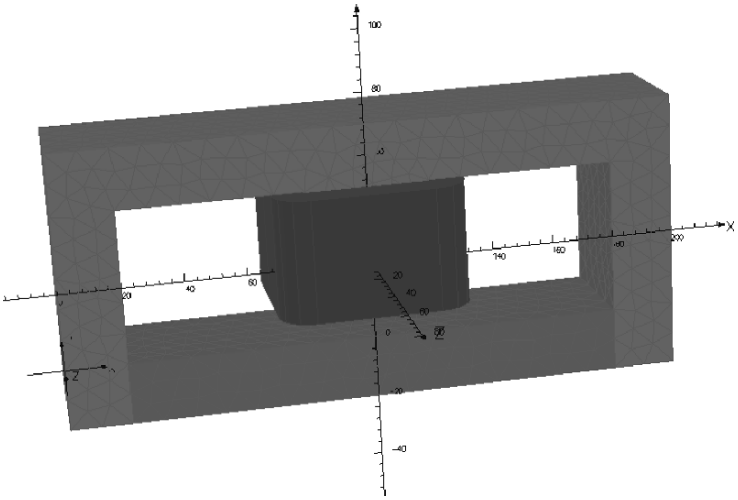

Fig. 4.10 3D finite-element mesh of the electromagnet (t = 10 mm)

width is comparable with the linear size of the central limb and a consequent leakage field can be noted.

Using the solid modelling technique, the model shown in Fig. 4.10 is obtained. From this model a three-dimensional mesh composed of about 250,000 tetrahedra has been generated. The depth of the magnetic core, in particular, has been taken equal to the square root of the cross-section of the central limb (30 mm).

The corresponding plot of computed vectors is shown in Fig. 4.11.

The force acting on the movable part of the electromagnet is computed too, by means of the Maxwell's stress tensor. A surface embedding the movable core is taken as the integration surface. The two models can be compared: in Fig. 4.12 the forces vs air-gap curves are shown for both two- and three-dimensional models.

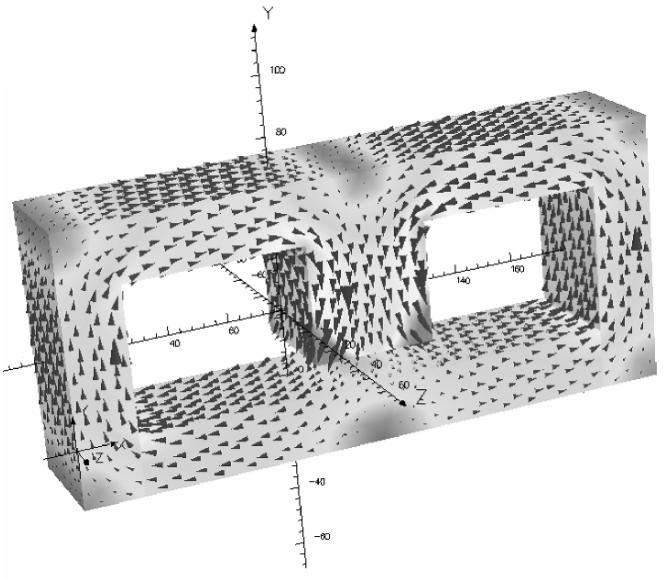

Fig. 4.11 Vector plot of magnetic induction (t = 10 mm, winding not shown)

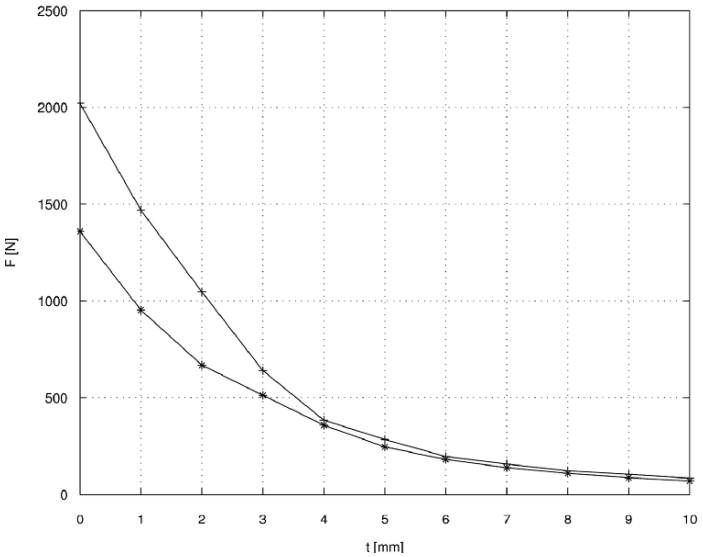

Fig. 4.12 Force vs air-gap curve (+2D, *3D)

The discrepancy between the two curves can be attributed to the leakage field in the z direction, that is neglected in the two-dimensional analysis. In principle, the three-dimensional analysis gives a more accurate prediction of the force. On the other hand, the remarkable increase of the number of elements, and so the computational cost, when passing from two to three dimensions, must be noted as well.